Numerical Thermoelastic Analysis of Complicating Factors in Optics Used in Laser Interferometers for Detection of Gravitational Waves

David Djambazov

Faculty Sponsor: Professor Rochus Vogt

Research Supervisor: Dennis Coyne

Final SURF Report 1996

LIGO T960185-00-D

18 Oct 96

Abstract:

Heating due to the high power of the laser beam required in the LIGO interferometer, creates thermal and thermoelastic deformations of the core optics (mirrors and beam-splitters). This leads to altering of the index of refraction “seen” by the laser beam, thus deforming it’s wave-front. Because of the very fine measurement required for the gravitational wave detection, it is important to bring the wave-front errors to a minimum. An analytical formulation was implemented for an idealized representation of the phenomenon and applied for the specifications of the LIGO core optics. Finite Element Models (FEM), which compared successfully against the analytical model, were extended to include factors not amenable to analysis -- wedge angle on the mirrors and non-normal incidence of the laser beam. The results obtained in the study indicate the amount of wave-front error due to thermal efforts, which is to be expected in LIGO. This will prove important, especially for advanced LIGO interferometers, when the laser power is increased.

Introduction:

The Laser Interferometer Gravitational-Wave Observatory (LIGO) project is the ambitious efforts of scientists from Caltech and MIT to create a facility capable of detecting cosmic gravitational waves. Some of the significant results expected to be obtained with help of LIGO include the first direct verification of the predictions of the General Theory of Relativity regarding the existence and the character of gravitational waves, as well as the first firm confirmation of the existence of exotic objects like black holes and naked singularities.

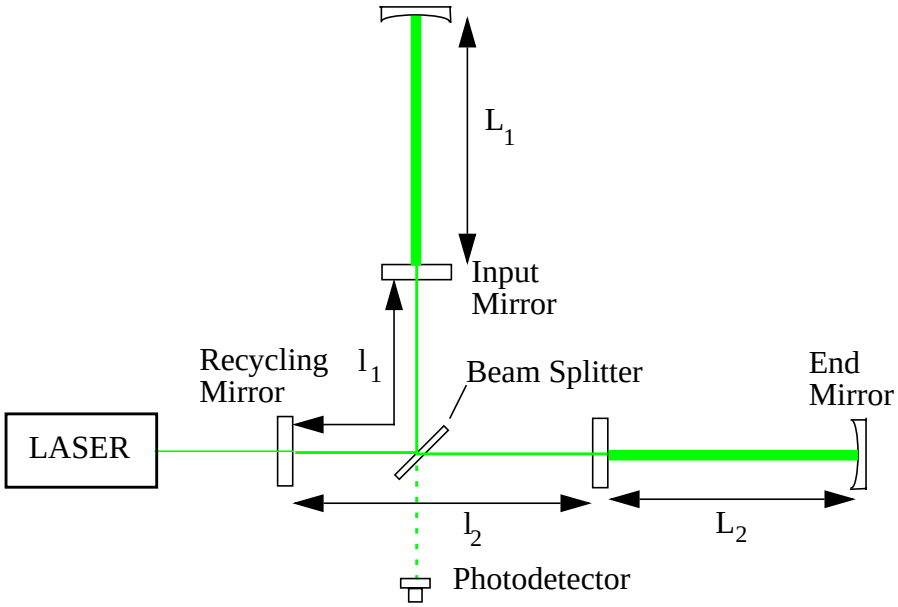

Figure 1: Basic Configuration

The idea behind the LIGO project is to use laser interferometry (see Figure 1) to measure strain caused by gravitational waves. Over the four kilometer baseline (L_1 and L_2) of the interferometer, the magnitude of the strain amplitude corresponds to actual change in length of 10^{-18} meters for initial LIGO detectors. Due to the precision of such measurement, the requirements for the laser beam are very demanding -- high power (about 10kW initially in the resonant cavities) and in the same time small wave-front error ($\lambda/800$). This especially applies to the Fabry-Perot cavities within which the trapped beam-light increases the power significantly. Absorption of part of the light energy in the coating and the bulk of the optics results in thermoelastic deformation and thermal lensing.

-Thermoelastic Deformation and its effect on the wave-front

Thermoelastic deformation can result in two effects: as wave-front distortion upon reflection and as change in cavity length (relaxation oscillator). As the high powered laser beam carries hundreds of watts of light power through the input mirror, within the cavity of long storage time, tens of kilowatts will be continuously reflected on its internal coated surface. Power dissipation in the coating and the substrate on the order of hundreds of milliwatts will produce temperature gradients, resulting in refraction index gradients and geometric alterations of the reflecting surface, thus distorting the wave-front. At the same time, the dissipated energy will bring about thermal changes in the cavity length -- an undesirable effect as it would cause a change in the phase of the beam, and possibly act as a relaxation oscillator.

-Thermal Lensing Effect

As most materials have a temperature dependence of their index of refraction, thermal lensing plays an important role in the wave-front distortion process. When the beam is transmitted through an optic piece, energy dissipation due to absorption along the way creates a temperature gradient which in turn gives rise to a gradient in the index of refraction in the heated volume. Thus the substrate acts as a lens and distorts the wave-front.

-Governing Equations:

To determine the governing equations it is necessary to understand the physical situation which we are trying to describe. In our case we have an optic suspended in vacuum on a very thin wire. Therefore the only influence on the test mass is the incoming beam flux, which means that the mirror would behave as a free mass. As a result there is no internal generation of heat in the case of absorption of power in the coatings, so the Fourier equation governs:

$$\rho C \frac{\delta T}{\delta t} - K \Delta T = 0$$

where $T(t,r,z)$ is the temperature distribution as a function of time (t), radial (r) and axial (z) coordinates; ρ is the density of the substrate; C is the specific heat; and K is the thermal conductivity.

For ease of computation, and since the temperature change is small, the nonlinear radiation boundary condition is linearized. The following expression for the radiative losses of a surface element at temperature *T* can be derived:

$$F = 4\sigma' T_0^3 \delta T$$

where T_0 is the ambient temperature, σ' -- Stefan-Boltzmann constant corrected for emissivity, and

$$\delta T = T - T_0$$

The other boundary condition is front surface absorption of a Gaussian beam.

In the case of heating by bulk absorption, the following equation governs due to internal heat absorption:

$$\rho C \frac{\delta T}{\delta t} - K \Delta T = \alpha I(r)$$

where α the attenuation coefficient and $I(r)$ is the irradiation intensity distribution (Gaussian).

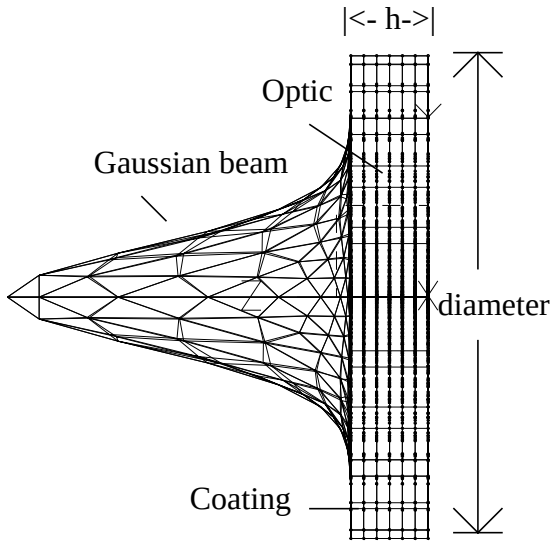

Figure 2: Schematic representation of the incoming Gaussian beam in the idealized case

-Analytical Formulation

An extensive treatment of the analytical formulation for both steady state solution and transient response of the system, has been published by the VIRGO project [1]. As the authors had treated also both cases of coating and in depth absorption, we decided it is best to employ their analytical treatment of the problem.

The solution is obtained as a summation of eigenvalues (fast converging Dini series) with coefficients given by the solution of a number of transcendental equations dependent upon geometry (radius and height of optic) and material properties (density, specific heat, and thermal conductivity).

The next step in the formulation is calculation of the effects of thermal lensing by analyzing the assumption that the local index of refraction is related to the local temperature in the following manner:

$$n(x, y, z) = n_0 + \frac{dn}{dT}[T(x, y, z) - T_0]$$

where n_0 is the reference index corresponding to the temperature T_0. Therefore the expression for the optical path distortion becomes:

$$\psi(r) = \frac{dn}{dT}\int_{-\frac{h}{2}}^{\frac{h}{2}}[T(r, z) - T_0]dz$$

In the above equation h is the thickness of the optic. Then finally the authors expand this expression for axisymmetric aberration on the basis of Zernike polynomials within the optical radius.

In a second article [2], the same authors present an analytic formulation for the case of thermoelastic deformations in an axisymmetric temperature field *T(t,r,z)*. The non-zero strain components of the strain tensor $\boldsymbol{E}$ are:

$$E_{rr} = \frac{\partial u_r}{\partial r}, \quad E_{\phi\phi} = \frac{u_r}{r}, \quad E_{zz} = \frac{\partial u_z}{\partial z}, \quad E_{rz} = \frac{1}{2}\left(\frac{\partial u_r}{\partial z} + \frac{\partial u_z}{\partial r}\right)$$

where $\boldsymbol{u}$ is the displacement vector. In the non-uniform temperature field the strain tensor $\boldsymbol{E}$ and the stress tensor, ϑ are related by:

$$\vartheta_{rr} = -\nu T + \lambda E + 2\mu E_{rr}$$

$$\vartheta_{\phi\phi} = -\nu T + \lambda E + 2\mu E_{\phi\phi}$$

$$\vartheta_{zz} = -\nu T + \lambda E + 2\mu E_{zz}$$

$$\vartheta_{rz} = 2\mu E_{rz}$$

where E is the trace of the strain tensor: $E = E_{rr} + E_{\phi\phi} + E_{zz}$.

The equilibrium equations for the stress tensor are:

$$\frac{\partial \vartheta_{rr}}{\partial r} + \frac{\partial \vartheta_{rz}}{\partial z} + \frac{\vartheta_{rr} - \vartheta_{\phi\phi}}{r} = \rho \frac{\partial^2 u_r}{\partial t^2}$$

$$\frac{\partial \vartheta_{rz}}{\partial r} + \frac{\partial \vartheta_{zz}}{\partial z} + \frac{\vartheta_{rz}}{r} = \rho \frac{\partial^2 u_z}{\partial t^2}$$

As there are no external forces, the boundary conditions reduce to:

$\vartheta_{rr}(a, z) = 0$, $\vartheta_{rz}(a, z) = 0$, $\vartheta_{rz}\left(r, \pm\frac{h}{2}\right) = 0$, $\vartheta_{zz}\left(r, \pm\frac{h}{2}\right) = 0$, where a is the radius of the optic.

The axially symmetric (Gaussian) light intensity distribution is expanded as a Dini Series on the basis of orthogonal Bessel functions. The result of further derivation is a fast converging Dini Series expansion used for obtaining a solution for $u_r(t, r, z)$ and $u_z(t, r, z)$, the radial and axial components of the displacement.

-Aim of project

From this point on we face the complexity of the non-idealized case where many different factors may affect the behavior of the system. The most important of these factors are wedge angles and non-normal beam incidence on the optics. The best way to gain practical knowledge about their magnitude and relevance is through a numerical simulation of perturbations in the idealized case. Furthermore, part of the motivation for the current study was the opportunity to apply the analytical formulation extensively for the LIGO optics specifications and determine the magnitude of the higher order Zernike terms of the wave-front expansion.

Simulation Methods:

The purpose of the project was to create a self consistent simulation of perturbations of the idealized case. Thus we first had to create an analytical model based on the analytical formulation from [1] and [2].

-Analytical model

We used ***Mathematica*** [3] for this part of the project. In the process of coding up we kept to the logical arrangement of the original papers, however we also did various additional calculations and comparison graphs based on the formulation.

The following flow-chart describes the process of creating the analytical model:

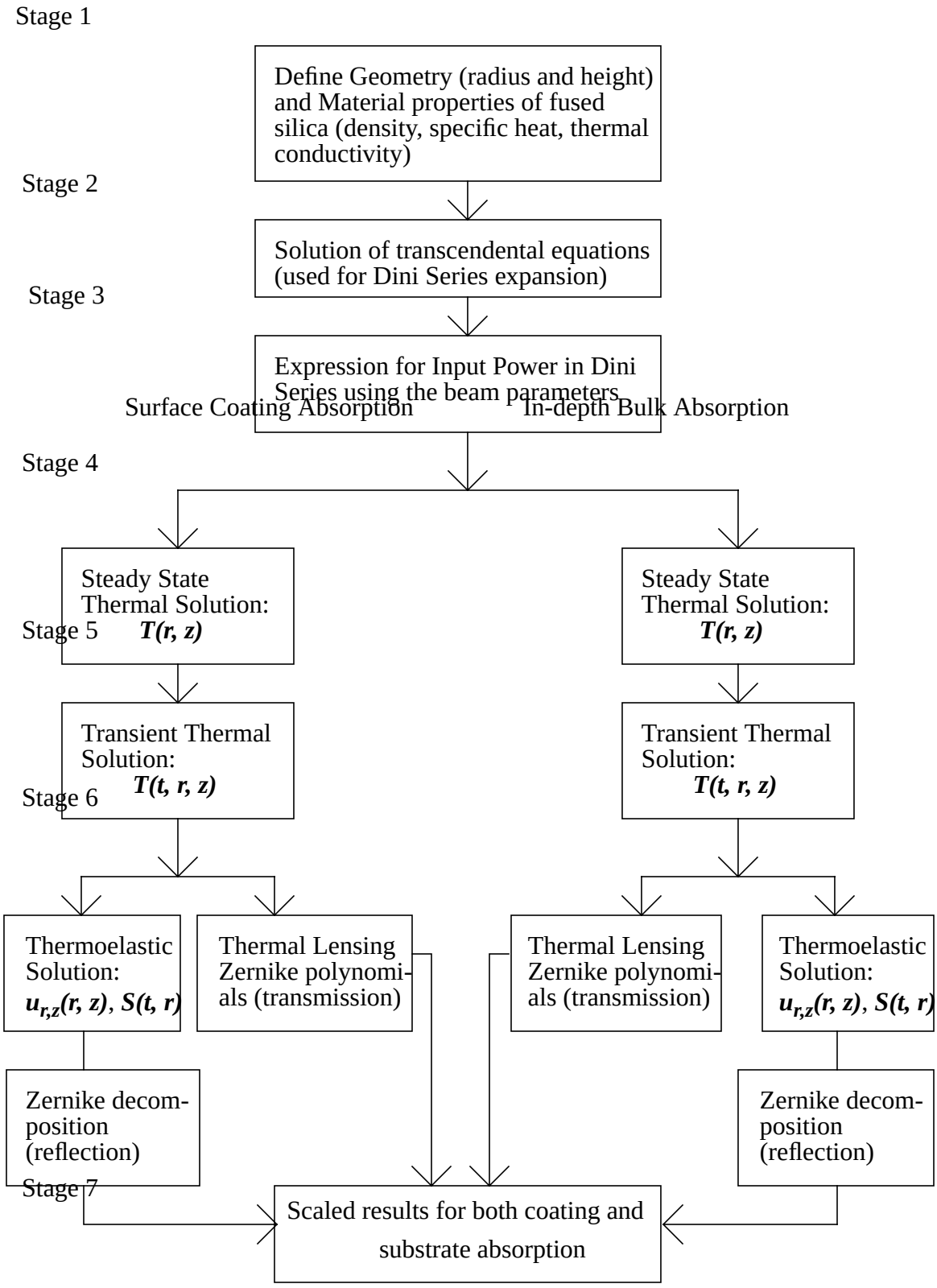

The seven stages of the flow-chart correspond to modules built within the ***Mathematica*** notebooks. The purpose of doing that was to enable easy rerun and clarity of the coded formulation. Thus the actual utilization of the analytical model had two main components: run and comparison against the original papers, using their values for the optic and the

beam, and run and comparison against the numerical model, using the LIGO specifications.

It is important to note that while the second stage is very time and resource consuming, it entirely depends upon the geometrical and material data of the given optic, so it has to be run only once for each different type of mirror. The rest of the factors (e.g. beam waist, beam power, etc.) can be easily changed and rerun for various conditions specified by the parameters involved in the calculation.

Since the equations are linear, the calculations are for the case of 1 Watt absorbed. At stage seven the results are scaled and added up together in a proper way, so that we can look at the figures for the combined effect of coating and in-depth absorption on resulting thermoelastic deflection (reflection) and thermal lensing (refraction).

-Comparison to published results

Along with the creation of the models it was very important to check the consitency of the calculation by comparing against the results published in papers [1] and [2]. So first we ran the constructed model for the numbers given in the original papers. The comparison shows very good agreement between the analytical formulation and the coded up analytical model as is evident from the figures:

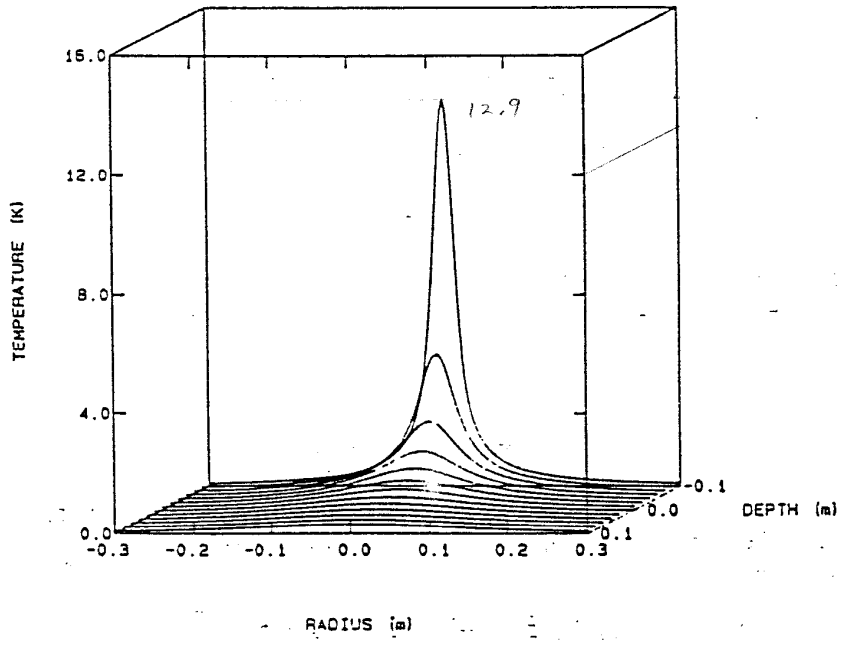

Figure 2: Thermal Steady State results for Absorption in the Coating (published result)

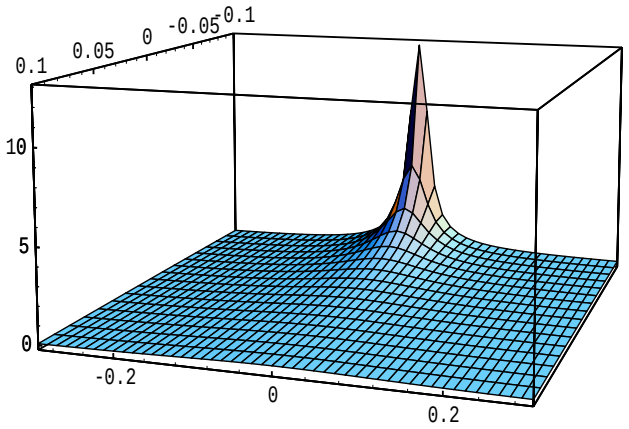

Figure 3: Thermal Steady State results for Absorption in the Coating (Analytical Model)

It is evident that for the considered steady state case the comparison for the temperature results reveals a very good agreement between the analytical model and formulation. This observation is furthermore confirmed by the transient behavior of the first few Zernike polynomials which very clearly converge to values close to the steady state values stated in the analytical formulation [1] and [2].

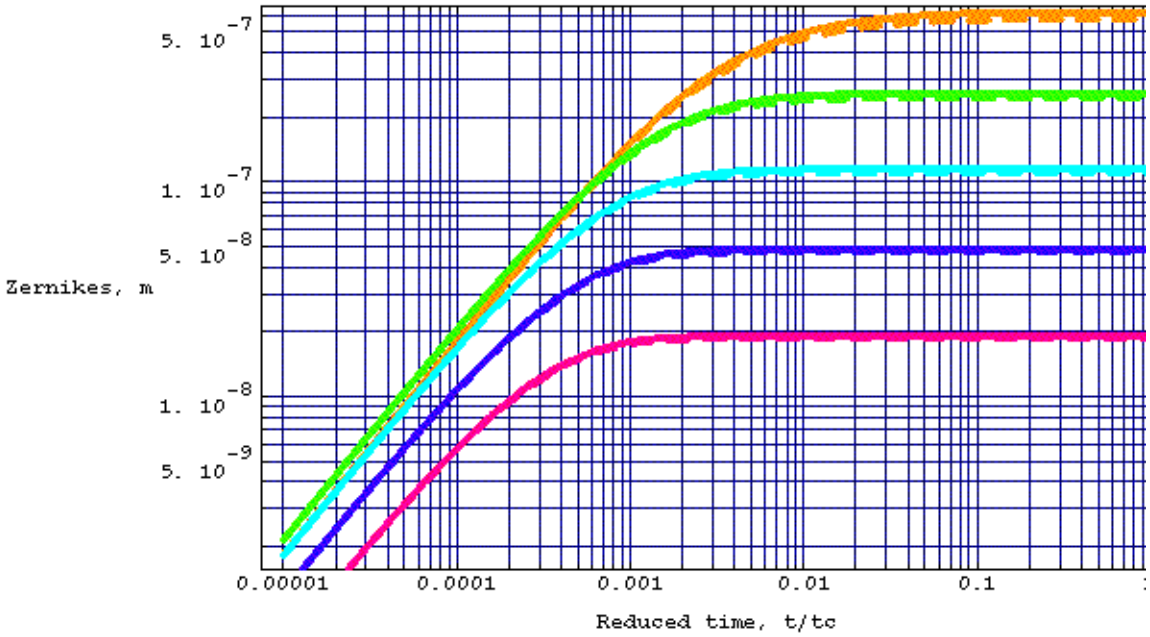

Figure 4: The transient behavior of the first five Zernike polynomials agrees very well with the results published by the VIRGO team and used for the analytical model

-Finite Element Model

The same basic assumptions used for the analytical part of the simulation were used for the construction of the Finite Element Models. The simulation software used was *Structural Dynamics Research Corp*.'s computer simulation package ***I-DEAS*** [4]. We created the simulation in five basic stages: optic geometry definition, meshing, definition of boundary conditions, model solution, and post processing of the results. First we considered the idealized case (same as the analytical model) of non-wedged cylindrical geometry, normal beam incidence, and axisymmetric Gaussian beam.

In the design stage we used the LIGO core optics specifications to construct the geometry of each individual optic. Next we meshed the geometrical model into 2592 linear, isoparametric, quadrilateral, three dimensional elements (3031 nodal points), radially increasing in element size (see Figure 4). The purpose of this particular type of mesh is to give more precision within the region most affected by thermal lensing and thermoelastic deformation. At this point we defined the material properties of the substrate (fused silica for all optics).

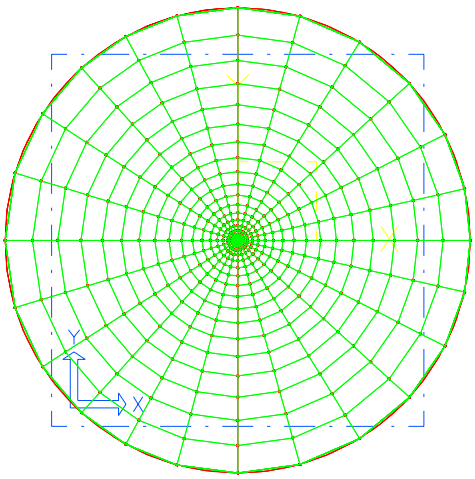

Figure 5: Geometry of the finite element mesh

The following step in the construction of the FEM was the definition of boundary conditions. We used the already stated assumptions to set the conditions of the simulation. The linearized form of the radiation equation allowed us to use convection, in order to simulate the effect. We calculated for amplitude of the constant convection coefficient of 5.72 Watts/K m^2 and ambient temperature of 293K. Then for the heat influx of the beam, we associated with one watt of absorbed power a Gaussian Data Surface described by:

$$f(r) = \frac{2P}{\pi w^2}\exp\left(-\frac{2r^2}{w^2}\right)$$

where P = 1 Watt, w is the beam waist, r is the radial coordinate of optic.

Then we ran the calculation for the temperature field under the given conditions for all of the LIGO core optics. After that stage we constructed a linear static model of the thermoelastic deformations using the results from the thermal analysis. At this point it turned

out that it is rather important to pick appropriate degrees of freedom (d.o.f.) so that the thermal expansion is not artificially constrained and yet the equations are not singular. The following figure illustrates our definition of the model's constrained d.o.f. (translational d.o.f. and three fixed points in cyan) :

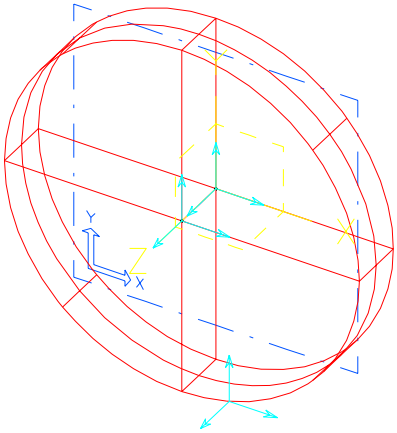

Figure 6: Degrees of Freedom defined with three fixed points and the translational d.o.f.'s associated with them

Once the proper boundary conditions were established we ran the linear static simulation and obtained results for the thermoelastic deformation. The whole simulation was then reiterated for all the LIGO core optics in the idealized case and compared against the analytical model results.

The last and most exciting part of the numerical simulation was of course the perturbation of the idealized case with the two main factors under consideration -- wedge angle and non-normal beam incidence. That was done by simply changing the geometry of the optic in the first stage of the FEM construction.

-Comparison to Analytical model

Before going on and analyzing the results of the simulation, it was very important to see how the FEM numerical results for the idealized case compare against the analytic model results, which were already determined to be consistent with the starting assumptions and the analytical formulation. As we decided that we will look most closely into the effects on the Beamsplitter for a number of reasons stated below, here is a comparison figure for the Beamsplitter idealized case:

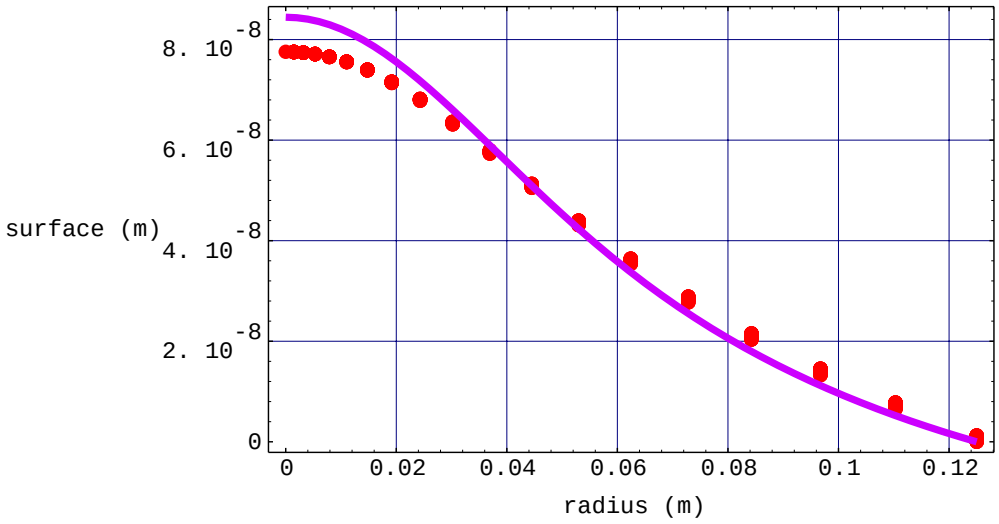

Figure 7: Thermoelastic Surface Displacement Comparison for the entire optic. The curve represents the Steady State analytical solution, while points correspond to node data from the Finite Element analysis. Results are for 1 Watt absorbed at the surface.

An even more interesting comparison is the decomposition into Zernike polynomials (Table 2). The results indicate a very good match between the analytical and the finite element models. There is a corresponding reasonable match of the peak-to-peak temperatures: 5.2K and 4.4K respectively for the analytical model and the FEM.

TABLE 1. Comparison of Zernike Decomposition within optical radius 5 cm for idealized Beamsplitter case (no wedge angle, normal beam incidence). Results are for 1 Watt absorbed power at the surface. Piston is not compared due to an ambiguity in the analytical formulation

No.	**U**	**Description/Eqn.**	**Analytical** (nm)	**Numerical** (nm)
6	U_2^0	Focus, $2\rho^2 - 1$	19.2	15.7
15	U_4^0	Spherical, $6\rho^4 - 6\rho^2 + 1$	-2.80	-1.72
28	U_6^0	$20\rho^6 - 30\rho^4 + 12\rho^2 - 1$	0.33	0.33
45	U_8^0	$70\rho^8 - 140\rho^6 + 90\rho^4 - 20\rho^2 + 1$	-0.03	0.19

LIGO Optics Parameters:

Prior to executing the simulation of the so constructed FEM's, we looked into the following table, describing the LIGO core optics, in order to get a preliminary idea of what would be the most interesting optic to concentrate on.

TABLE 2. Scaling table of optics and their specifications

Parameter	Recycling Mirror	Beam Splitter	Input Test Mass	End Test Mass
Thickness (meters)	0.10	0.04	0.10	0.10
Beam Waist (meters)	0.037	0.0515	0.0365	0.046
Incident Power (Watts)	6/180[a]	360/180	180/9000	9000
Coating Absorptivity (ppm)	1	1	1	1
Substrate Absorption (ppm/cm)	20	2	2	-
Maximum Wedge Angle (degrees)	3	1	3	3
Diameter (meters)	0.125	0.125	0.125	0.125

a. Two different figures for the incident power indicate that the beam going through that optic enters a resonant cavity. The first number is the beam power entering the cavity, and the second -- the resonant power inside of it (Transmission/Reflection).

Since results are calculated on a per Watt absorbed basis, they are dependent only upon the geometry of the optic and the laser beam waist. Consequentially, we expect the RM, ITM and ETM to respond similarly. Furthermore, the remaining optic -- the Beamsplitter is the thinnest of all, and is the only one exposed to both the effects of wedge angle and 45 degree of beam incidence. All of these factors inclined us to focus our efforts on getting results, for the perturbed case, pertaining to the Beamsplitter.

Results:

Taking into account the estimated magnitude of the studied effects on each mirror as represented in the scaling table, we decided to split the results for both the analytical and the finite element models into two parts -- Beamsplitter results and a summary table for the rest of the LIGO core optics.

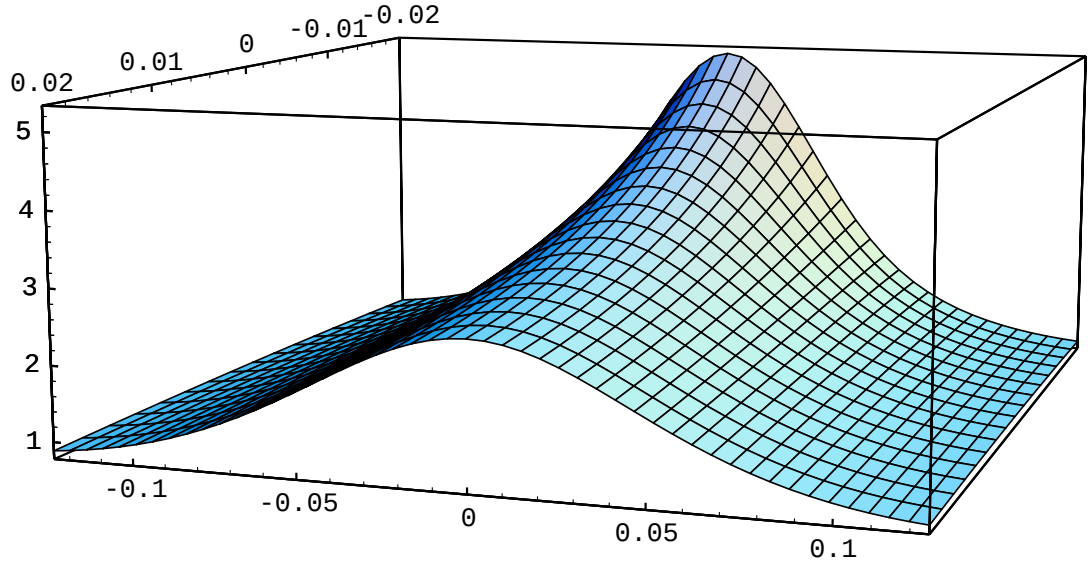

Figure 8: Representation of the temperature field for the steady state of 1 Watt absorption in the coating of the Beamsplitter (non-wedged, normal incidence case)

First let's look into the analytical results. Figures 8 and 9 represent the steady state temperature field solutions for the two separate cases of coating and in-depth absorption. As we demonstrated earlier the results are convergent and agree to a considerable extent with the results obtained in the earlier studies, which we used for our analytical formulation. It is evident that absorption in the coating leads to a higher increase in temperature as well as higher gradients than in-depth absorption.

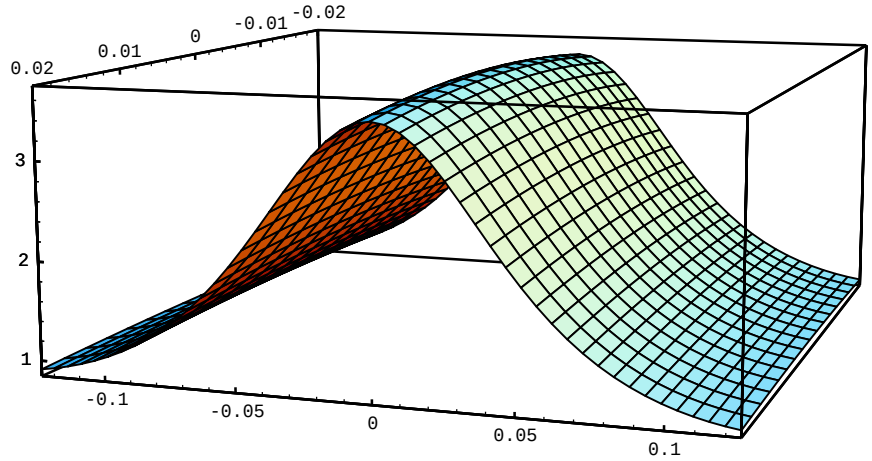

Figure 9: Representation of the temperature field for the steady state of 1 Watt in-depth absorption for the Beamsplitter

Next we calculated the effect of thermoelastic deformation resulting from the increase in temperature. Figure 10 represents the peak-to-peak amplitude of the deformation for the entire radius of the Beamsplitter. We noticed that the absorption in the coating accounts

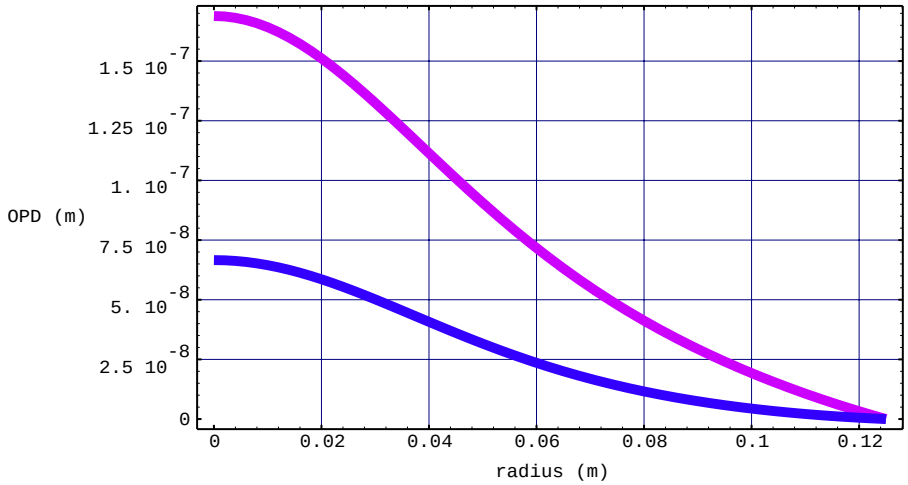

Figure 10: Optical Path Difference for Thermoelastic Deformation -- comparison of coating versus in-depth absorption for the entire radius of the Beamsplitter for 1 Watt absorbed. Violet curve represents the effect of coating absorption, and blue curve -- the same effect for the in-depth case

for an effect twice as big as the effect caused by absorption in the substrate.

For thermal lensing, however, we observed that the magnitude of the Optical Path Difference is almost identical for the cases of in-depth and coating absorption as can be seen in Figure 11. Note that since ***dn/dt*** is positive for fused silica (11.8 ppm/K), the thermal lens is a converging lens; the optical path is larger at the center than at the periphery.

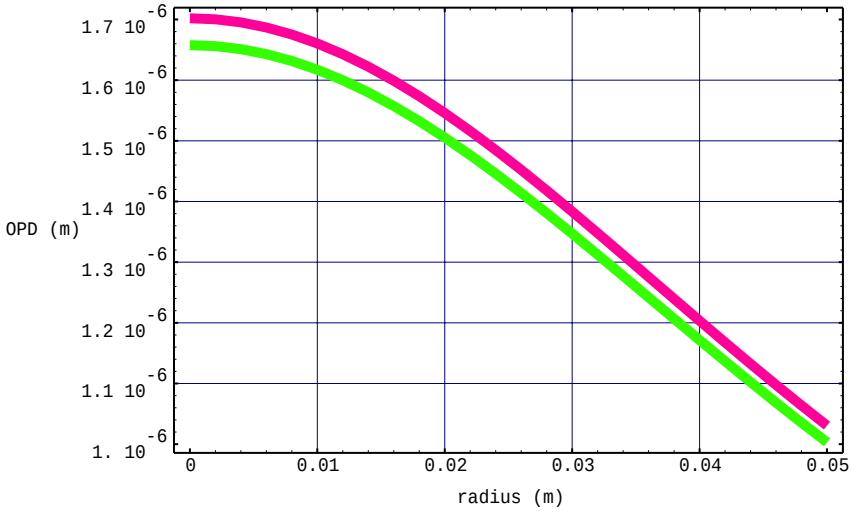

Figure 11: Optical Path Difference for Thermal Lensing -- comparison of coating versus in-depth absorption of 1 Watt for the entire radius of the Beamsplitter. Red curve represents coating absorption, and green curve corresponds to in-depth absorption.

In our analytical analysis of thermoelastic deformation and thermal lensing we decompose the results into Zernike polynomials which describe quantitatively the different aberrations of the wave-front, which in our case happen to be unwanted wave-front errors. So for the purposes of LIGO it is very important to look at a scaled table of the first few Zernike polynomials for all the optical elements in the case of surface absorption, which as we saw either dominates or equals the case of in-depth absorption.

TABLE 3. Summary of results for Surface Absorption

Quantity		**RM**	**ITM**	**ETM**	**BS**
	Limits to Absorption, ppm transmission/reflection	<40 / <50	<40 / <2	NA / < 4	<20 / < 50
Thermal Lensing (Transmission)	Wavefront P-V, nm	9.9	19.8	30.1	5.9
	Z2 (focus), nm	-4.7	-9.4	-14.7	-2.9
	Z4 (spherical), nm	1.1	2.3	2.6	0.5
	Z6, nm	-0.2	-0.5	-0.4	-0.1
Thermoelastic Deflection (Reflection[a])	Wavefront P-V, nm	0.54	1.09	3.41	0.76
	Z2 (focus), nm	0.52	1.04	1.63	0.35
	Z4 (spherical), nm	-0.12	-0.25	-0.28	-0.05
	Z6, nm	0.03	0.05	0.04	0.01

a. values are for the reflected wavefront, i.e. twice the surface values.

The results in Table 3 are scaled for the specified absorption limits, the initial LIGO power levels and apply over the central 10 cm diameter region.

-Finite Element Model results for LIGO core optics

As we already mentioned, our main interest in the finite element no-wedged, normal beam incidence model was to verify the consistency of our simulation method with the analytical model constructed before the FEM. Therefore relying on the data from Figure 7 and on the peak temperature result we can confidently say that our finite element simulation method is reasonable and consistent with the nature of the considered physical system.

So now we can look onto the simulation of the most interesting case of the combination of complicating factors: 1 degree wedge angle and 45 degree beam incidence for the Beamsplitter. We considered only the case of Surface Absorption as we saw it yielded the most interesting (maximal) values for all the parameters we calculate. The maximum value of the temperature field is about 4.7K -- slightly lower than the analytical idealized steady state case, but still higher than for the finite element analysis of the idealized geometry. In the same time this is the right place to mention that we observed an elliptical isothermal pattern on the front surface, as opposed to the concentric circles in the case of the non-wedged, normal beam incidence case.

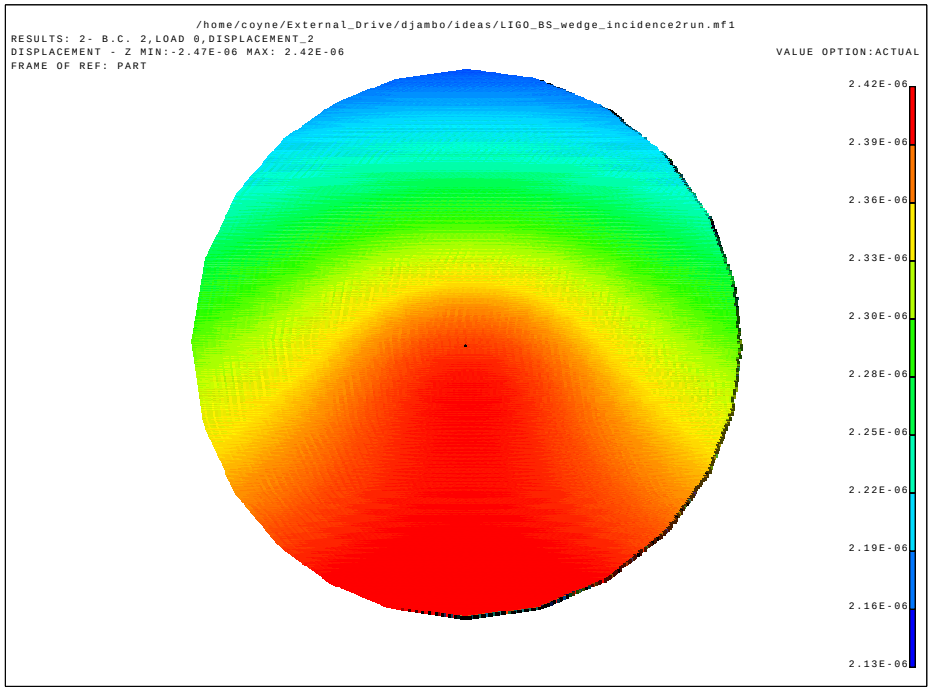

Figure 12: Surface deformation for wedged, 45 degree beam incidence case of the Beamsplitter. The result is calculated for 1 Watt absorption in the coating.

What we were really interested in was to see how the complicating factors are going to affect the surface deformation of the Beamsplitter. This is exactly what Figure 12 shows us. We observed a non-axisymmetric aberration of the surface at the thick end of the edge

(red part of graph). Clearly the biggest effect of the wedge and non-normal incidence is non-axisymmetric Zernike terms, as Table 4 shows.

-Post Processing of results

To post process the results we exported the values of the deformation in the Z-direction for all the nodes of the finite element model to ***Mathematica*** for Zernike decomposition and obtained the following table for the thermoelastic deformation:

TABLE 4. Zernike Comparison for Thermoelastic Deformation for 1 Watt Surface Absorption

Zernike term	FEA, non-wedged, normal incidence (nm)	FEA, 1 degree wedge, 45 degree incidence (nm)	Analytical Model, non-wedged, normal incidence (nm)
Tip	0.02	1.20	~
Tilt	0.00	-51.1	~
X-astigmatism	0.00	4.7	~
Y-astigmatism	0.00	0.13	~
Focus	-15.7	-17.1	-19.2
X-coma	0.024	0.095	~
Y-coma	0.002	0.021	~
Spherical	1.71	1.15	2.8

Clearly the X-astigmatism term is significant relative to the focus term for the wedged, 45 degree beam incidence FEM result. Especially significant are the tip and the tilt. The Analytical Model results naturally project only axisymmetric terms, while the FEM of the same geometry demonstrates near zero values in those and thus once again confirming the validity of our results.

Discussion:

The results of this study will be used to generate phase maps of wave-front error which are analyzed in an electromagnetic field propagation analysis of the LIGO resonant optical cavities to determine the effect on performance. The total allowable wave-front errors (due to polishing errors, coatings, birefringence and thermal effects) are given in the Core Optics Components Design Requirements Document [5]. These requirements express limits on the allowable wave-front error within spatial frequency bands, so that a one-to-one comparison with the above results is not immediately possible. However, in general, the requirements are as follows (in the central region of the optic surface):

- Reflection (on the surface): < ~2 nm rms (after removing piston, tilt and focus components of the error)
- Reflection (on the surface): focus error < ~32 nm p-v
- Reflection (on the surface): BS astigmatism < 16 nm surface p-v
- Transmission: < ~11 nm rms for the BS and < ~21 nm rms for the other COCs (after removing piston, tilt and focus components of the error)

In all cases the thermal contributions to the overall allowable wave-front error are less than the requirements. However, the thermal components are in some cases significant. In par-

ticular, for advanced LIGO designs, thermal effects will be necessitate improved, low absorption coatings (and improved contamination control).

Conclusion:

Over the course of this project we developed analytical and finite element tools for simulation and analysis of thermally induced wave-front error, which we proved to confirm some of the effects predicted by published studies, given the same problem conditions and assumptions. In the same time however our simulation method permits analysis of factors not amenable to analytical formulation in a consistent and not too time consuming process. We used these tools to analyze factors pertaining to the parameters of LIGO and concluded that these factors can affect the advanced stages of LIGO and thus we put into a clearer frame one of the many technical challenges of LIGO.

References:

[1] Hello P. and Vinet J. Y., ***Analytical models of thermal aberrations in massive mirrors heated by high power laser beams*** - *J. Phys. France* 51 (1990) 1267-1282.

[2] Hello P. and Vinet J. Y., ***Analytical models of transient thermoelastic deformations of mirrors heated by high power cw laser beams*** - *J. Phys. France* 51 (1990) 2243-2261.

[3] Wolfram S., ***Mathematica: A System for Doing Mathematics by Computer****, version 2.2, 2nd ed.* Addison-Wesley Pub. Co., 1991.

[4] ***I-DEAS Master Series 2, Solid Modeling and Simulation Program****, Structural Dynamics Research Corp.,* 1996.

[5] Kells W., ***Core Optics Components Requirements (1064 nm)***, LIGO-E950099-02-D, 1/29/96.